ACS APPLIED MATERIALS & INTERFACES

Research Article

www.acsami.org

Functional Built-In Template Directed Siliceous Fluorescent Supramolecular Vesicles as Diagnostics

Jie Li,[†,#] Kaerdun Liu,[†,#] Hengyu Chen,[‡,#] Ruoyan Li,[‡] Markus Drechsler,[§] Fan Bai,[*,‡] Jianbin Huang,[*,†] Ben Zhong Tang,[*,∥] and Yun Yan[*,†]

[†]Beijing National Laboratory for Molecular Sciences (BNLMS), College of Chemistry and Molecular Engineering and [‡]Biodynamic Optical Imaging Center (BIOPIC), School of Life Sciences, Peking University, Beijing 100871, China

[§]University of Bayreuth, Bayreuth, D-95440, Germany

[∥]Department of Chemistry, Division of Biomedical Engineering, Hong Kong Branch of Chinese National Engineering Research Center for Tissue Restoration and Reconstruction, the Hong Kong University of Science & Technology, Clear Water Bay, Kowloon, Hong Kong, China

Supporting Information

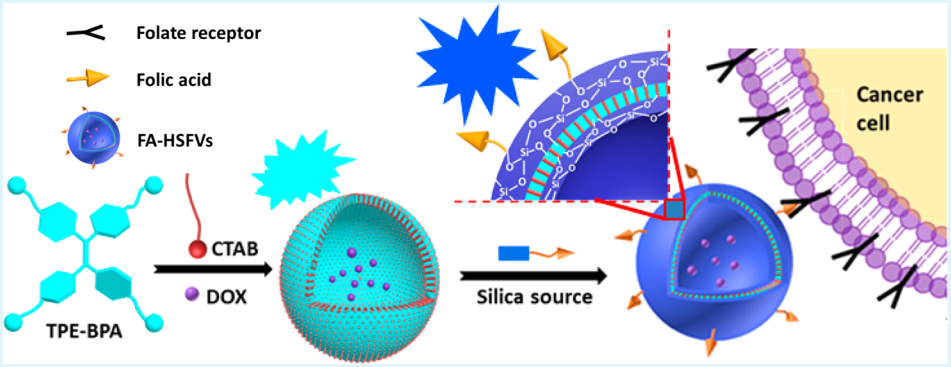

ABSTRACT: Functional template directed synthesis of hybrid siliceous fluorescent vesicle (HSFV) is fabricated by using fluorescent vesicle as a built-in template. The template vesicle is the ionic self-assembly of an aggregation-induced emission (AIE) fluorogen. Upon depositing folic acid modified silica shell on its surface, the obtained HSFVs display low cytotoxicity, significant fluorescence, and targeted drug delivery toward cancer cells. Furthermore, the wall-thickness of the HSFVs can be controlled via altered concentration of silica source. This is the first report of HSFV employing the template vesicle as a built-in fluorescent agent, which represents a good example of rational design for an effective diagnostics, and may open up a new avenue for precision medicine.

KEYWORDS: *hybrid self-assembly, aggregation-induced emission, template, fluorescent vesicles, precision medicine*

INTRODUCTION

Currently, one important objective within the field of precision medicine is to develop diagnostics with targeting functions.[1−6] Owing to their versatility, mainly supramolecular self-assemblies are employed to fabricate various diagnostics. Supramolecular assemblies are often made with synthetic polymers with desired functional blocks, such as the fluorescent block, responsive block, and targeting block. Drugs are usually loaded in the core of supramolecular self-assemblies (micelles or vesicles), and are delivered to the diseased sites for a therapy.[7−14] Recently, self-assemblies based on drug/biomolecule multiple components are also invented,[15,16] which allow combining the chemotherapy and imaging components into one nanoplatform.[17,18] Although diagnostics made with molecular assemblies are facile to prepare, they often suffer from problems of stability and biocompatibility in the human physiological environment.

On the other hand, diagnostics based on silica nanoparticles are also employed for storage of active molecules owing to their excellent biocompatibility and stability.[19−22] However, the fabrication of silica based diagnostics is very tedious, usually involving multiple steps like fabrication of template, template synthesis of silica nanoparticles, removal of the template, and functionalizing of silica nanoparticles.[23−26] Especially, the template is often sacrificial, and does not offer any function to the obtained silica nanoparticles. As a result, various functional groups, such as imaging,[27] targeting,[28] and controlled releasing,[29] have to be attached to the silica nanoparticles step by step. All these efforts add up to a tremendous workload, which not only reduces the yield of production, and increases

Received: May 5, 2017
Accepted: June 15, 2017
Published: June 15, 2017

DOI: 10.1021/acsami.7b06306
ACS Appl. Mater. Interfaces 2017, 9, 21706−21714

Scheme 1. Illustration of Self-Assembly of TPE-BPA@8CTAB Vesicles, Preparation of Folic Acid Modified Silicated Fluorescent Supramolecular Vesicles (FA-HSFVs), and Their Targeted Combination with Cancer Cells[a]

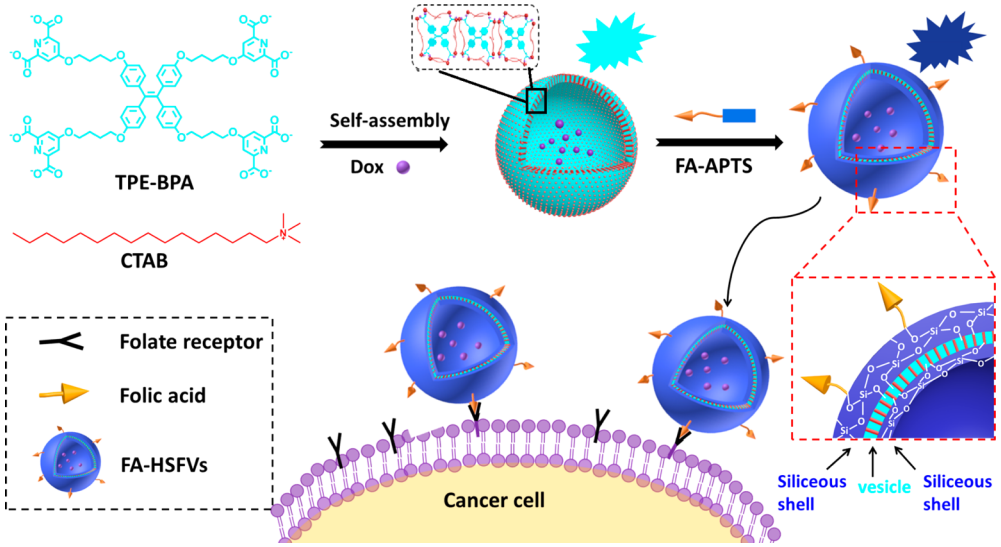

[a]FA-HSFVs are conveyed to the cancer cell due to the specific interaction between folate receptor and folic acid.

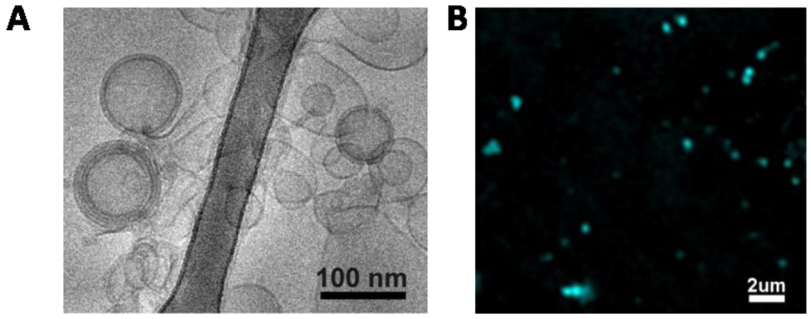

Figure 1. (A) Cryo-TEM images of TPE-BPA@8CTAB vesicles. (B) CLSM image of TPE-BPA@8CTAB vesicles. [TPE-BPA] = 100 μM, [CTAB] = 800 μM.

the risk of cytotoxicity, but also decreases the number density of each functional group due to limited available surface area.[30]

To avoid these problems, herein we report an unprecedented functional template directed synthesis of hybrid siliceous fluorescent vesicles (HSFVs) with integrated ability for fluorescent imaging, drug-loading, cancer-cell targeting, and controlled rate of drug release. Fluorescent supramolecular vesicles displaying dual functions of imaging and drug loading are used as templates to induce the hydrolysis of folic acid modified silica source. Since the template is not removed, the obtained vesicles immediately become targeting fluorescent diagnostics (nanodrugs if drugs are loaded) toward cancer cells. Moreover, the thickness of the silica shell can be fine-tuned by controlling the concentration of the silica source, thus allowing the desired rate of drug release. Since the imaging and targeting groups are located at the supramolecular layer and the silicate layer of the HSFVs, respectively, it enables dual high efficiency of imaging and targeting toward cancer cells. Furthermore, dialysis separation of the unloaded drug is not needed since centrifugation can result in sedimentation of the siliceous vesicles loaded with drug, which can be readily dispersed again under gentle vortex or sonication for a few seconds. This work shows that upon integrating supramolecular vesicles and silica nanocarriers into one platform, we are able to develop advanced hybrid diagnostics facilely, which can even combine therapeutic ability by loading drugs. We expect that combination of supramolecular self-assembly of aggregation induced emission molecules with silica particles will provide a promising strategy for the new generation of nanodrug.

RESULTS AND DISCUSSION

The fluorescent supramolecular vesicles are prepared through ionic self-assembly of a propeller-shaped molecule TPE-BPA (Scheme 1) which displays aggregation induced emission (AIE). Different from conventional planar fluorescent dyes exhibiting a notorious aggregation-caused quenching effect, AIE dyes are not emissive in a free motion state but strongly emissive when aggregating as a result of restricted vibration.[31−35] The unique light-up behavior has enabled them to be promising biolabels and visualizing agents.[36−38] TPE-BPA was synthesized in our lab.[39] This molecule contains the tetraphenylethene (TPE) group, which is the typical AIE moiety.[40−42] The design of eight negative charges allows formation of ionic supramolecular vesicles TPE-BPA with positively charged amphiphiles in water. As cetyltrimethylammonium bromide (CTAB) was added to the aqueous solution of TPE-BPA, optimal fluorescent vesicles were formed at the charge neutral molar ratio of TPE-BPA:CTAB = 1:8, as reported in our previous work.[43] These vesicles were formed as a result of hydrophobic interaction between the supramolecular

DOI: 10.1021/acsami.7b06306
ACS Appl. Mater. Interfaces 2017, 9, 21706−21714

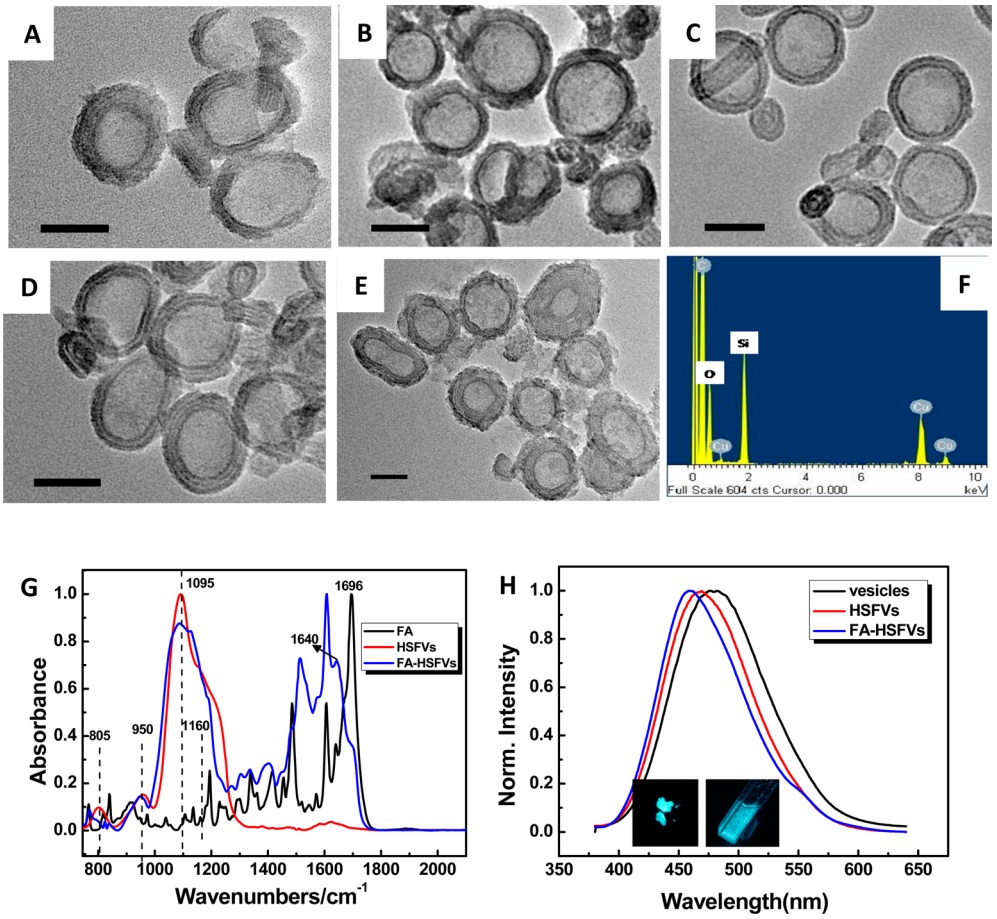

Figure 2. (A–E) TEM images of HSFVs made with [TEOS] = 22.4 μL/mL (A), [TEOS] = [FA-APTS] = 11.2 μL/mL (B), [TEOS] = 6.72 μL/mL (C), [TEOS] = 8.95 μL/mL(D), and [TEOS] = 56.0 μL/mL (E); scale bar = 50 nm. (F) EDX result of the HSFV. (G) FT-IR spectra for the HSFVs/FA-HSFVs (red line). The blue and black lines are the FT-IR spectra for folic acid (FA) modified HSFV (FA-HSFV) and the FA, respectively. (H) Fluorescent spectra of TPE-BPA@8CTAB solution and the suspension of HSFVs/FA-HSFVs. Inset in (H): photo of centrifuged sediments (left) and suspension in water (right) of HSFVs under 365 nm UV lamp.

block of TPE-BPA@8CTAB, which was discussed in detail in our previous work. Figure 1A,B shows the cryo-transmission electron microscopy (cryo-TEM) and confocal laser scanning microscopy (CLSM) image of the supramolecular TPE-BPA@8CTAB vesicles, respectively.

Hybrid siliceous fluorescent vesicles (HSFVs) were generated upon introducing tetraethoxysilane (TEOS) and folic acid modified (3-aminopropyl)triethoxysilane (FA-APTS), into the aqueous system of TPE-BPA@8CTAB supramolecular vesicle under vigorous stirring. Fluorescent suspension was obtained after 24 h at pH = 5.6. Fluorescent sediments can be obtained upon centrifugation of this suspension at 10 000 rpm for 15 min. The sediments were readily dispersed into water upon 30 s sonication. SEM (Figure S1) observation reveals the formation of spherical particles with diameters about 80–100 nm. These spherical particles, without staining on the sample, are found to be multilamellar vesicles under TEM (Figure 2A,B), featuring the presence of inorganic components in the vesicular shell. We speculate that a silica shell has been deposited in both the inner and outer surfaces of each single TPE-BPA@8CTAB membrane, since the silica source may interact with the polar head of this membrane via hydrogen or electrostatic interaction. This conclusion can be verified by the equally high contrast of the vesicle wall at both the inner and outer surfaces. The diameter of these silicate vesicles is about 80 nm, which is the same as the size of the multilamellar supramolecular vesicles of TPE-BPA@8CTAB in Figure 1A. It is noticed that some of the vesicles can be broken under sonication, indicating the silicate layers are fragile. In the latter, we may find that the fragile feature of the vesicles facilitates release of entrapped drugs.

The morphologies of the vesicles are not noticeably different as the silica source varied from TEOS to the mixture of TEOS/FA-APTS (1/1, molar ratio, Figure 2B, and Figure S2), except that the number of walls differs a little bit. For vesicles silicated with TEOS, the number of vesicle walls is about 4–6, whereas that can be 2–6 when silication is carried out with TEOS/FA-APTS. It is possible that the bulky FA-APTS is against the formation of a homogeneous silica layer. Indeed, when all the TEOS was replaced with FA-APTS, the silication process failed. The maximum molar fraction of FA-APTS for successful fabrication of folic acid modified siliceous vesicle was 0.5, so that the 1/1 mixture of TEOS/FA-APTS was employed throughout this study to ensure high folic acid grafting on the surface of the silica vesicles.

The preformation of TPE-BPA@8CTAB supramolecuar vesicles is very crucial in leading to well-defined HSFVs (Figure S3). Uniform and regular hollow structures are only observed at the molar ratio of TPE-BPA:CTAB around 1:8 where well-defined vesicles are formed. Amorphous structures

DOI: 10.1021/acsami.7b06306
ACS Appl. Mater. Interfaces 2017, 9, 21706–21714

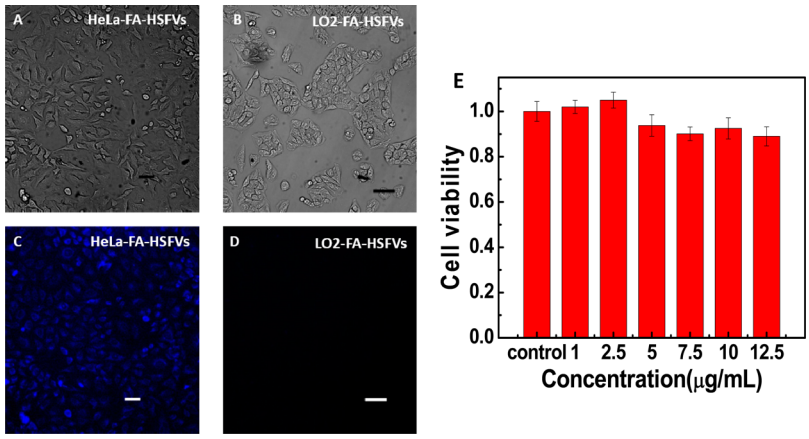

Figure 3. CLSM images of cells with nanocarriers: bright field images of HeLa (A) and LO2 (B) cells with FA-HSFVs; fluorescence images of HeLa (C) and LO2 (D) cells with FA-HSFVs. The concentrations of FA-HSFVs were 10 μg/mL. Scale bar = 25 μm. (E) Cytotoxicity of FA-HSFVs with different concentrations in HeLa cells.

are produced when CTAB is deficient, such as at the molar ratio of TPE-BPA/CTAB = 1:4; whereas numerous small nanoparticles (10 nm) are observed in excess of CTAB (TPE-BPA/CTAB = 1:12). This fact, together with the multilamellar structure of the HSFVs and their similar size to the TPE-BPA@8CTAB vesicles, clearly manifests that the supramolecular vesicle of TPE-BPA@8CTAB acts as template for the growth of SiO_2 shells.

Furthermore, pH also has great impact on the siliceous vesicle formation (Figure S4). The optical pH range is around 5.0−6.0. High or low pH resulted in amorphous and polydispersed structures, presumably due to the fast hydrolysis process prohibiting duplicating the vesicular structure very well.[44]

The wall-thickness of the HSFVs can be controlled by varying the concentration of the silica source. With increasing the concentration of TEOS from 6.72 μL/mL to 8.95, 22.4, and 56.0 μL/mL, the obtained wall-thickness was 6.5 ± 1.2, 8.3 ± 1.3, 9.9 ± 2.9, and 12.1 ± 4.2 nm, respectively (Figure 2C−E and Figure S5 for analysis of the wall thickness).

EDX measurement (Figure 2F) verifies the presence of the element Si and O in the sediments, and their molar ratio is about 1:2. Furthermore, FT-IR spectrum (Figure 2G) displays the characteristic strong asymmetric vibration of Si−O−Si at 1095−1160 cm^{-1}, and symmetric vibration of SiO_4 network at 805 cm^{-1}, confirming the formation of SiO_2. The presence of a weak vibration at 950 cm^{-1} indicates there are also some Si−OH groups in the silicate layer.[45] All these results support the formation of hybrid siliceous fluorescent vesicles (HSFVs). Notice that the IR spectra show an obvious peak corresponding to carbonyl amide group (1640 cm^{-1}) for the HSFVs prepared with TEOS/FA-APTS (1:1) (which is denoted as FA-HSFV in Figure 2), whereas this peak is absent for those obtained from mere TEOS, indicating the successful grafting of folic acid on the hybrid FA-HSFVs.

The silication of the supramolecular vesicles has remarkable influence on the fluorescence (Figure 2H). The emission peak of the HSFVs (467 nm) and FA-HSFVs (458 nm) is blue-shifted compared to that for the native TPE-BPA@8CTAB vesicles (479 nm), suggesting that deposition of SiO_2 on the TPE-BPA@8CTAB vesicle has strongly twisted the TPE-BPA molecules.[46] It is possible that the polar outer layer of the TPE-BPA@8CTAB vesicles (including the CTA^+, COOH, and COO^- groups) has interacted with the polar groups from the silica source generated in the process of hydrolysis of TEOS or FA-APTS. Both hydrogen bonding and electrostatic interaction may occur, which changes the configuration of the TPE-BPA molecules in the hydrophobic domain of the vesicles. Obviously, the introduction of FA-APTS to the silica shell has twisted the TBE-BPA molecules to a stronger extent, which is featured by the much bluer emission. However, FA-APTS does not affect the stability of the HSFVs. The size and morphology for both the bare HSFVs and FA-HSFVs are not changed even after one year, revealing their superior stability (Figure S6). Furthermore, the macroscopic appearance of the FA-HSFVs (and also the bare HSFVs without folic acid modification) is powder after drying the sediments, which is very convenient for their storage and further application.

The imaging and targeting ability of the FA-HSFVs was investigated by incubating the HeLa cells (human cervical cancer cell line) and LO2 cells (human normal hepatic cell line) in the presence of FA-HSFVs. Blue fluorescence from cytoplasm of HeLa cells was observed after 24 h (Figure 3C). In clear contrast, the fluorescence is extremely weak for LO2 cells (Figure 3D), indicating the excellent targeting ability of the FA-HSFVs to cancer cells. Meanwhile, control experiment (Figure S7, the CLSM made with HSFVs) validates that the targeting ability is from folic acid groups, because HSFVs without FA shows only faint fluorescence in HeLa cells (and LO2 cells). Since folic acid receptors are highly expressed on the surface of tumor cells,[47−49] this distinct targeting ability clearly manifests the successfully grafting of folic acid groups on the surface of the FA-HSFVs.

Cytotoxicity of the unloaded FA-HSFVs was evaluated using a typical (3-4,5-dimethyl-2-thiazolyl)-2,5-diphenyl-2-*H*-tetrazolium bromide (MTT) colorimetric bioassay.[50,51] Figure 3E shows that the cell viabilities within 24 h for living HeLa cells are all higher than 90% as the daily doses ranging from 0 μg/mL (control) to 12.5 μg/mL, indicative of negligible cell toxicity of the empty FA-HSFVs. This result is extremely amazing, since CTAB on its own is known to show severe instant cell toxicity.[52] Obviously, the diffusion of CTAB molecules in the hybrid vesicles have been doubly blocked by the silica shell and the ionic self-assembly, which makes the FA-HSFVs quite promising for in vitro diagnostic applications.

To study the drug loading and releasing ability of the FA-HSFVs, Doxorubicin hydrochloride (DOX), a fluorescent dye and water-soluble anticancer drug, was loaded into the TPE-

DOI: 10.1021/acsami.7b06306
ACS Appl. Mater. Interfaces 2017, 9, 21706−21714

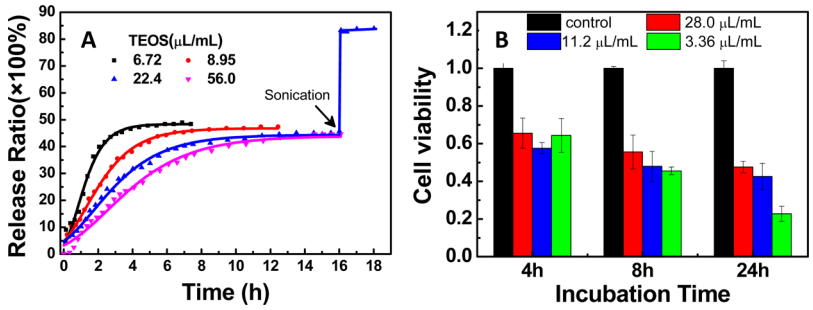

Figure 4. (A) DOX releasing profile of HSFVs with different amounts of TEOS at pH = 5.5, 37 °C. The releasing efficiency can be over 80% after 10 min sonication. The legends represent the amount of TEOS added during the preparation of HSFVs. [TEOS] = 6.72, 8.95, 22.4, and 56.0 μL/mL. (B) Cell viability of HeLa Cells incubated with DOX loaded FA-HSFVs over time. The cell viability decreases with lowering the concentration of the silica source. The concentration of FA-HSFVs is 10 μg/mL. The legends represent the amount of TEOS added during the preparation of DOX-loaded FA-HSFVs. [TEOS] = [FA-APTS] = 28.0, 11.2, and 3.36 μL/mL, T = 37 °C.

BPA@8CTAB supramolecular vesicles. In a typical procedure, the hydrophilic DOX was added into water where the ionic self-assembly of TPE-BPA@8CTAB vesicles can occur. Then there must be some DOX be entrapped in the vesicles, which would remain there during the following silication process. Then separation of the unloaded DOX from the loaded ones was made simply via centrifugation. Since this facile procedure avoids dialysis, dialysis triggered drug leaking is prohibited so that it allows high DOX loading efficiency of 21−23%. Specifically, fluorescence resonance energy transfer (FRET)[53,54] between DOX and the TPE-BPA molecules was observed before silication (Figure S8, the emission of TPE-BPA is 479 nm, which is in good agreement with the excitation of DOX (477 nm)[55]). Whereas the phenomenon of FRET disappeared after depositing silica on the TPE-BPA@8CTAB vesicles to fabricate HSFVs/FA-HSFVs (Figure S8), which can be explained by the mismatch of the dipole orientation of the TPE-BPA and DOX caused by the silication triggered twisting of the TPE-BPA molecule.

Significantly, the release rates of DOX from the HSFVs are closely related to the wall-thickness (Figure 4A). The thicker the wall is, the slower the release rate becomes. For systems prepared with the concentration of TEOS being 6.72, 8.95, 22.4, and 56.0 μL/mL, the corresponding wall-thickness of HSFVs is 6.5 ± 1.2, 8.3 ± 1.3, 9.9 ± 2.9, and 12.1 ± 4.2 nm, respectively. In line with the increased wall-thickness, the time required to reach the releasing equilibrium also increases. Figure 4A shows that the releasing equilibrium can be reached within 2.8, 6.0, 8.8, and 11.8 h, respectively.

The overall fraction of released DOX from the HSFVs displays pH dependent behavior. At pH 5.5, about 40−50% DOX was released at equilibrium (Figure 4A), whereas it was lowered to 35−45% at pH 7.0 (Figure S9). This is mainly due to the increased hydrophilicity and solubility of DOX at higher pH, because the $-NH_2$ groups on DOX can be protonated at acidic pH, which increases the solubility of DOX.[56] Since pH 5.5 is often the internal environment of cancer cells,[57] the present results indicate that the HSFVs have higher release rate in cancer cells. Usually, the drug released from a nanocarrier is below 70% due to the interaction of drugs with nanocarriers.[58] However, in the present study, the released DOX can be further promoted to over 80% upon imposing pulse of sonication for 10 min. This sonication enhanced release rate is independent of pH (Figure 4A, blue curve), because breaking of the rigid wall of HSFVs/FA-HSFVs may occur (Figure 2A). Since sonication has been clinically applied in therapy,[59] the FA-HSFVs represent a novel family of highly efficient releasing system.

Figure 4B shows the efficiency of DOX loaded in the FA-HSFVs in killing HeLa cells. In general, gradual decrease of the cell viability is observed for systems with different shell thickness, indicating a sustained release of DOX from all these FA-HSFVs. Significantly, the effect of wall thickness on the drug release becomes evident after 8 h. A drastic difference is observed within 24 h; by then the highest cell-killing rate can amount to 80% for FA-HSFVs with the thinnest wall thickness of 6.5 ± 1.2 nm. In contrast, the killing rates are about 60% for those FA-HSFVs with thicker walls. This result suggests that the present strategy allows design of nanocarriers with desired drug release rate for therapy of cancers at different development stage, which is very useful in view of practical application.

CONCLUSION

In summary, the strategy of built-in functional template directed synthesis of hybrid siliceous vesicles is very promising in facile preparation of multifunctional diagnostics. We show in this work that using the fluorescent vesicles as a built-in template, hybrid diagnostics with enhanced cyto-compatibility, sufficient fluorescence, efficient targeting, and facile drug loading can be obtained through a one-pot approach. Since different functions are expressed at the supramolecular part and the silica part of the hybrid vesicles, respectively; it allows facile integration of multiple desired functions at one platform without lowering their efficiency. We expect that the strategy of built-in functional template directed synthesis of siliceous nanoparticles opens a new vista in the field of precision medicine.

EXPERIMENTAL SECTION

Materials. TPE-BPA was synthesized according the previous report.[43] Cetyltrimethylammonium bromide (CTAB) was used after recrystallization for five times. Tetraethoxysilane (TEOS, AR) was purchased from Xilong Chemical Co., Ltd. Folic acid (FA, >97%) was purchased from Sigma-Aldrich. 3-Aminopropyltriethoxysiliane (APTES, >98%) and *N*-hydroxysuccinimide (NHS) were purchased from Tokyo Chemical Industry Co., Ltd. *N*,*N*′-Dicyclohexylcarbodiimide (DCC) was purchased from Sinopharm Chemical Reagent Co., Ltd. DMSO-d_6 (99.9%) was purchased from Cambridge Isotope Laboratories, Inc. Aqueous solutions were prepared using Milli-Q water of 18 MΩ.

Synthesis of Folic Acid-Modified (3-Aminopropyl)triethoxysilane (FA-APTS). The ^{1}H NMR experiments were performed on a Bruker ARX 400 MHz spectrometer with DMSO-d_6 as solvent. Mass

DOI: 10.1021/acsami.7b06306
ACS Appl. Mater. Interfaces 2017, 9, 21706−21714

Scheme 2. Synthesis of Folic Acid-Modified (3-Aminopropyl)triethoxysilane (FA-APTS)

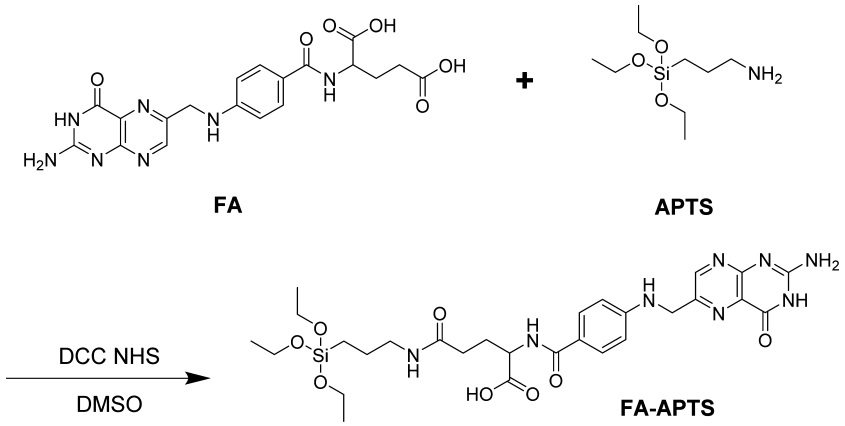

spectrum was determined on Bruker APEX IV Fourier Transform Ion Cyclotron Resonance Mass Spectrometer.

Folic acid (0.40 g, 0.91 mmol) was dissolved in 50 mL DMSO under 35 °C. *N*-Hydroxysuccinimide (NHS, 0.208 g, 1.81 mmol) and *N,N′*-dicyclohexylcarbodiimide (DCC, 0.372 g, 1.80 mmol) were added and the reaction was allowed in the dark under 35 °C for 48 h. After floating objects (*N,N′*-dicyclohexylurea, DCU) were filtered from the reaction system, trimethylamine (0.183 g, 1.81 mmol) and 3-aminopropyltriethoxysiliane (APTS, 0.400 g, 1.88 mmol) were added into the filtrate. The reaction was allowed for 8 h, and system was filtered to obtain clear yellow solution. Solid product was obtained by adding acetonitrile into DMSO (DMSO:acetonitrile = 1:2, volume ratio) (Scheme 2). Then the product was washed by acetonitrile 2 times, and dried in vacuum to give yellowish-white powder (FA-APTS, yield 20%).

^{1}H NMR (400 MHz, DMSO-d_6): 8.64 (s, 1H), 7.62 (s, 2H), 6.89 (s, N-1H), 6.61 (s, 2H), 4.47 (s, 2H), 4.35 (s, 1H), 3.71 (m, 6H), 2.33 (s, 2H), 2.08 (s, 2H), 1.40 (s, 2H), 1.09 (t, 9H), 0.52 (s, 2H). 2H was missing due to overlay with DMSO residue signal around 2.5.

High resolution MS (negative mode): 643.26479. Molecular formula $C_{28}H_{40}N_8O_8Si$, ion formula $C_{28}H_{39}N_8O_8Si$ [M-H], err 2.8 ppm.

Preparation of HSFVs and FA-HSFVs. Fluorescent vesicles were obtained by mixing TPE-BPA and CTAB in water with a molar ratio of 1:8 (100 μM:800 μM), where the pH was 5.6 ± 0.1, and then the vesicle solution was kept for 2 days at 25 °C. TEOS (100 mM) was added into the vesicle solution and the mixture was violently stirred for 24 h at 30 °C to give whitish fluorescent suspension. Upon centrifugation at a speed of 10 000 rpm for 15 min, fluorescent sediments (HSFVs) were obtained, which were washed for three times before use. The preparation of FA-HSFVs is the same as HSFVs except that only TEOS (100 mM) was replaced with the mixture of TEOS (50 mM)+FA-APTS (50 mM). The silicate vesicle sediments are yellow in this case. The shell thickness of HSFVs or FA-HSFVs was related to the amount of TEOS or the mixture of TEOS and FA-APTS.

Characterization of HSFVs and FA-HSFVs. Scanning electron microscopy (SEM) was performed on a Hitachi S4800 microscope. Transmission electron microscopy (TEM) images were recorded with a JEM-2100 instrument at an acceleration voltage of 200 kV. For SEM and TEM measurements, a drop of suspension (dispersed into distilled water) was placed on clean silicon sheets and carbon-coated copper grids and dried in the air, respectively.

Cryogenic transmission electronic microscope (Cryo-TEM) observation was performed on EM922 EFTEM (Zeiss NTS GmbH, Oberkochen, Germany). A few microliters of samples were placed on a bare copper TEM grid (Plano, 600 mesh), and the excess liquid was removed with filter paper. This sample was cryo-fixed by rapidly immersing into liquid ethane cooled to −170 to −180 °C in a cryo-box (Carl Zeiss NTS GmbH). The specimen was inserted into a cryo-transfer holder (CT3500, Gatan, Munich, Germany) and transferred to a Zeiss EM922 EFTEM. Examinations were carried out at temperatures around −180 °C. The TEM was operated at an acceleration voltage of 200 kV. Zero-loss filtered images were taken under reduced dose conditions (500−2000 e/nm^2). All images were recorded digitally by a bottom-mounted CCD camera system (UltraScan 1000, Gatan) and processed with a digital imaging processing system (Digital Micrograph 3.9 for GMS 1.4, Gatan).

Ultraviolet−visible (UV−vis) spectral measurements were performed on a Shimadzu UV-1800 spectrophotometer. Fluorescence (FL) measurements were carried out using a Hitachi F-4500 instrument. Fourier transform infrared (FT-IR) spectra were recorded with a Bruker Vector-22 spectrophotometer. Fluorescence images were recorded on Ti−S Nikon inverse fluorescence microscopy. Energy dispersive X-ray (EDX) measurements were performed on FEI Tecnai G2 T-20 transmission electron microscope. Quantitation method is Cliff Lorimer thin ratio section. All elements were analyzed (Normalized).

Cell Experiments. *Cell Culture.* HeLa cell lines were generous gifts, courtesy of Yujie Sun (Peking University, Beijing, China), routinely cultured in Dulbecco's modified Eagle's medium (Gibco, Grand Island, NY, USA) supplemented with 10% (v/v) fetal bovine serum (Hyclone, Logan City, UT, USA), 100 U/mL of penicillin, and 100 μg/mL of streptomycin (Gibco, Grand Island, NY, USA) at 37 °C in a humidified incubator containing 5% CO_2. LO2 cell lines were generous gifts, courtesy of Junlong Zhang (Peking University, Beijing, China), routinely cultured in RPMI-1640 (Gibco) supplemented with the same components as described above.

Cell Imaging. HeLa cells or LO2 cells were grown overnight in 35 mm Petri dishes. The nanocarriers (HSFVs, FA-HSFVs) were respectively transferred into the medium, immediately incubated with cells at 37 °C at a dose of 10 μg/mL. Wells with cells without test compound (but with equal proportion of sterile PBS) were included as controls. After a 24 h incubation, the cells were imaged under an inverted fluorescence optical microscope (Nikon, ECLIPSE Ti; λ_{ex} = 405 nm for nanocarriers; fluorescent signals were collected at 405 nm). The images of the cells were captured using a photomultiplier.

Cytotoxicity Assay of Nanocarriers in Vitro. MTT assay was employed to measure the cell viability. As an indicator system of cytotoxicity, MTT assay has been reported to exhibit equal or even higher precision than [^{3}H] thymidine incorporation assay.[60,61] As the intensively colored formazan sediments metabolized by MTT clearly reflect cell respiration, the amount of sediments is proportional to the level of cell viability. Therefore, cytotoxicity can be measured by obvious differences in quantified cell survival. 5 × 10^3 HeLa cells were seeded into a 96-well plate per well, which were incubated overnight at 37 °C in a 5% CO_2 atmosphere. Then, various doses of 0−12.5 μg/mL unloaded carriers (i.e., FA-HSFVs) were transferred into the aforementioned medium, immediately incubated at 37 °C. Including wells with medium without cells or nanoparticles, cells without test compound (but with equal proportion of sterile water) were used as controls. After 24 h incubation, 10 μL of MTT solution (5 mg/mL in

DOI: 10.1021/acsami.7b06306
ACS Appl. Mater. Interfaces 2017, 9, 21706−21714

PBS) was added into each well. After further incubation for 4 h, 150 μL of DMSO was added to dissolve the formazan sediments. The cell survival rate was quantified by the optical density readings at 490 nm taken with a plate reader. Every experiment was performed 6 times.

Doxorubicin Loading and Cell Viability Assay in Vitro. Doxorubicin (DOX)-loaded HSFVs and FA-HSFVs was prepared by a one-pot procedure: TPE-BPA, DOX, and CTAB (100 μM:100 μM:800 μM) were mixed together in water at pH = 5.6 at 25 °C and the solution was kept at 25 °C in the dark for 48 h. Then TEOS or the mixture of TEOS and FA-APTS was added. After violently stirring for 24 h at 30 °C, a red suspension were obtained. Upon centrifugation at 10 000 rpm for 15 min, red solids, which are the DOX loaded HSFVs or FA-HSFVs, were obtained. Then the solids were washed with water several times to remove the adsorbed DOX. UV−vis spectra were used to track whether the adsorbed DOX was removed entirely. All the experiments were carried out in the dark to avoid photodamage of DOX.

The encapsulation percentage of DOX was determined with UV−vis scanning spectrophotometry at 480 nm in water according to the calibration curve of different DOX concentrations. The DOX loading efficiency = (amount of loaded DOX/amount of total DOX) × 100%. For DOX-loaded HSFVs, the loading efficiency was 19.1%, 21.3%, 19.1%, and 16.0% corresponding to TEOS of 6.72, 8.95, 22.4, and 56.0 μL/mL, respectively. For DOX-loaded FA-HSFVs, the loading efficiency was 22.7%, 21.8%, and 21.2% corresponding to TEOS+ FA-APTS of 6.72, 22.4, and 56.0 μL/mL, respectively. (The molar ratio of TEOS:FA-APTS = 1:1.)

In cell viability assay, the DOX-loaded FA-HSFVs with different thicknesses were transferred into the medium, and immediately incubated with HeLa cells at 37 °C at a dose of 10 μg/mL. Including wells with medium without cells or nanoparticles, cells with equal proportion of sterile water without test compound were used as controls. After 4, 8, and 24 h, the cell viability was tested by MTT assay, as described above. Each assay was repeated 12 times.

■ ASSOCIATED CONTENT

Supporting Information

The Supporting Information is available free of charge on the ACS Publications website at DOI: 10.1021/acsami.7b06306.

SEM images of HSFVs, TEM images of FA-HSFVs, Preparation conditions of HSFVs, Stability of HSFVs and FA-HSFVs, Thickness analysis of HSFVs (PDF)

■ AUTHOR INFORMATION

Corresponding Authors

*E-mail: fbai@pku.edu.cn.
*E-mail: jbhuang@pku.edu.cn.
*E-mail: tangbenz@ust.hk.
*E-mail: yunyan@pku.edu.cn.

ORCID

Ben Zhong Tang: 0000-0002-0293-964X
Yun Yan: 0000-0001-8759-3918

Author Contributions

#Jie Li, Kaerdun Liu, and Hengyu Chen contributed equally.

Notes

The authors declare no competing financial interest.

■ ACKNOWLEDGMENTS

This work is supported by the National Natural Science Foundation of China (Grant No. 21573011, 21422302), National Basic Research Program of China (2013CB933800), and the Innovation and Technology Commission of Hong Kong (ITC−CNERC14S01).

■ REFERENCES

(1) Warthaka, M.; Adelmann, C. H.; Kaoud, T. S.; Edupuganti, R.; Yan, C.; Johnson, W. H.; Ferguson, S.; Tavares, C. D.; Pence, L. J.; Anslyn, E. V.; Ren, P.; Tsai, K. Y.; Dalby, K. N. Quantification of a Pharmacodynamic ERK End Point in Melanoma Cell Lysates: Toward Personalized Precision Medicine. *ACS Med. Chem. Lett.* **2015**, *6*, 47−52.

(2) Lin, M. M.; Kim, H.-H.; Kim, H.; Dobson, J.; Kim, D. K. Surface Activation and Targeting Strategies of Superparamagnetic Iron Oxide Nanoparticles in Cancer-Oriented Diagnosis and Therapy. *Nanomedicine* **2010**, *5*, 109−133.

(3) Ramogida, C. F.; Orvig, C. Tumour Targeting with Radiometals for Diagnosis and Therapy. *Chem. Commun.* **2013**, *49*, 4720−4739.

(4) Cho, H.-S.; Dong, Z.; Pauletti, G. M.; Zhang, J.; Xu, H.; Gu, H.; Wang, L.; Ewing, R. C.; Huth, C.; Wang, F.; Shi, D. Fluorescent, Superparamagnetic Nanospheres for Drug Storage, Targeting, and Imaging: A Multifunctional Nanocarrier System for Cancer Diagnosis and Treatment. *ACS Nano* **2010**, *4*, 5398−5404.

(5) Bardhan, R.; Lal, S.; Joshi, A.; Halas, N. J. Theranostic Nanoshells: From Probe Design to Imaging and Treatment of Cancer. *Acc. Chem. Res.* **2011**, *44*, 936−946.

(6) Kumar, R.; Shin, W. S.; Sunwoo, K.; Kim, W. Y.; Koo, S.; Bhuniya, S.; Kim, J. S. Small Conjugate-Based Theranostic Agents: An Encouraging Approach for Cancer Therapy. *Chem. Soc. Rev.* **2015**, *44*, 6670−6683.

(7) Caldorera-Moore, M. E.; Liechty, W. B.; Peppas, N. A. Responsive Theranostic Systems: Integration of Diagnostic Imaging Agents and Responsive Controlled Release Drug Delivery Carriers. *Acc. Chem. Res.* **2011**, *44*, 1061−1070.

(8) Al-Jamal, W. T.; Kostarelos, K. Liposomes: From a Clinically Established Drug Delivery System to a Nanoparticle Platform for Theranostic Nanomedicine. *Acc. Chem. Res.* **2011**, *44*, 1094−1104.

(9) Puri, A.; Blumenthal, R. Polymeric Lipid Assemblies as Novel Theranostic Tools. *Acc. Chem. Res.* **2011**, *44*, 1071−1079.

(10) Cabral, H.; Nishiyama, N.; Kataoka, K. Supramolecular Nanodevices: From Design Validation to Theranostic Nanomedicine. *Acc. Chem. Res.* **2011**, *44*, 999−1008.

(11) Liu, Y.; Feng, L.; Liu, T.; Zhang, L.; Yao, Y.; Yu, D.; Wang, L.; Zhang, N. Multifunctional pH-Sensitive Polymeric Nanoparticles for Theranostics Evaluated Experimentally in Cancer. *Nanoscale* **2014**, *6*, 3231−3242.

(12) Musyanovych, A.; Landfester, K. Polymer Micro- and Nanocapsules as Biological Carriers with Multifunctional Properties. *Macromol. Biosci.* **2014**, *14*, 458−477.

(13) Sun, C.-Y.; Shen, S.; Xu, C.-F.; Li, H.-J.; Liu, Y.; Cao, Z.-T.; Yang, X.-Z.; Xia, J.-X.; Wang, J. Tumor Acidity-Sensitive Polymeric Vector for Active Targeted siRNA Delivery. *J. Am. Chem. Soc.* **2015**, *137*, 15217−15224.

(14) Zhang, Z.; Ma, R.; Shi, L. Cooperative Macromolecular Self-Assembly toward Polymeric Assemblies with Multiple and Bioactive Functions. *Acc. Chem. Res.* **2014**, *47*, 1426−1437.

(15) Cheetham, A. G.; Zhang, P.; Lin, Y.-a.; Lock, L. L.; Cui, H. Supramolecular Nanostructures Formed by Anticancer Drug Assembly. *J. Am. Chem. Soc.* **2013**, *135*, 2907−2910.

(16) Baler, K.; Michael, R.; Szleifer, I.; Ameer, G. A. Albumin Hydrogels Formed by Electrostatically Triggered Self-Assembly and Their Drug Delivery Capability. *Biomacromolecules* **2014**, *15*, 3625−3633.

(17) Song, X.; Liang, C.; Gong, H.; Chen, Q.; Wang, C.; Liu, Z. Photosensitizer-Conjugated Albumin−Polypyrrole Nanoparticles for Imaging-Guided In Vivo Photodynamic/Photothermal Therapy. *Small* **2015**, *11*, 3932−3941.

(18) Chen, Q.; Wang, X.; Wang, C.; Feng, L.; Li, Y.; Liu, Z. Drug-Induced Self-Assembly of Modified Albumins as Nano-theranostics for Tumor-Targeted Combination Therapy. *ACS Nano* **2015**, *9*, 5223−5233.

(19) Argyo, C.; Weiss, V.; Bräuchle, C.; Bein, T. Multifunctional Mesoporous Silica Nanoparticles as a Universal Platform for Drug Delivery. *Chem. Mater.* **2014**, *26*, 435−451.

DOI: 10.1021/acsami.7b06306
ACS Appl. Mater. Interfaces 2017, 9, 21706−21714

(20) Tang, F.; Li, L.; Chen, D. Mesoporous Silica Nanoparticles: Synthesis, Biocompatibility and Drug Delivery. *Adv. Mater.* **2012**, *24*, 1504−1534.
(21) Vivero-Escoto, J. L.; Huxford-Phillips, R. C.; Lin, W. Silica-Based Nanoprobes for Biomedical Imaging and Theranostic Applications. *Chem. Soc. Rev.* **2012**, *41*, 2673−2685.
(22) Kim, J.; Kim, H. S.; Lee, N.; Kim, T.; Kim, H.; Yu, T.; Song, I. C.; Moon, W. K.; Hyeon, T. Multifunctional Uniform Nanoparticles Composed of a Magnetite Nanocrystal Core and a Mesoporous Silica Shell for Magnetic Resonance and Fluorescence Imaging and for Drug Delivery. *Angew. Chem., Int. Ed.* **2008**, *47*, 8438−8441.
(23) Wu, S.-H.; Mou, C.-Y.; Lin, H.-P. Synthesis of Mesoporous Silica Nanoparticles. *Chem. Soc. Rev.* **2013**, *42*, 3862−3875.
(24) Mackowiak, S. A.; Schmidt, A.; Weiss, V.; Argyo, C.; von Schirnding, C.; Bein, T.; Bräuchle, C. Targeted Drug Delivery in Cancer Cells with Red-Light Photoactivated Mesoporous Silica Nanoparticles. *Nano Lett.* **2013**, *13*, 2576−2583.
(25) Liu, J.; Hartono, S. B.; Jin, Y. G.; Li, Z.; Lu, G. Q.; Qiao, S. Z. A Facile Vesicle Template Route to Multi-Shelled Mesoporous Silica Hollow Nanospheres. *J. Mater. Chem.* **2010**, *20*, 4595−4601.
(26) Hartono, S. B.; Gu, W.; Kleitz, F.; Liu, J.; He, L.; Middelberg, A. P. J.; Yu, C.; Lu, G. Q.; Qiao, S. Z. Poly-l-lysine Functionalized Large Pore Cubic Mesostructured Silica Nanoparticles as Biocompatible Carriers for Gene Delivery. *ACS Nano* **2012**, *6*, 2104−2117.
(27) Kumar, R.; Roy, I.; Ohulchanskyy, T. Y.; Goswami, L. N.; Bonoiu, A. C.; Bergey, E. J.; Tramposch, K. M.; Maitra, A.; Prasad, P. N. Covalently Dye-Linked, Surface-Controlled, and Bioconjugated Organically Modified Silica Nanoparticles as Targeted Probes for Optical Imaging. *ACS Nano* **2008**, *2*, 449−456.
(28) Wang, Y.; Huang, R.; Liang, G.; Zhang, Z.; Zhang, P.; Yu, S.; Kong, J. MRI-Visualized, Dual-Targeting, Combined Tumor Therapy Using Magnetic Graphene-Based Mesoporous Silica. *Small* **2014**, *10*, 109−116.
(29) He, D.; He, X.; Wang, K.; Cao, J.; Zhao, Y. A Light-Responsive Reversible Molecule-Gated System Using Thymine-Modified Mesoporous Silica Nanoparticles. *Langmuir* **2012**, *28*, 4003−4008.
(30) Cauda, V.; Schlossbauer, A.; Kecht, J.; Zürner, A.; Bein, T. Multiple Core−Shell Functionalized Colloidal Mesoporous Silica Nanoparticles. *J. Am. Chem. Soc.* **2009**, *131*, 11361−11370.
(31) Luo, J.; Xie, Z.; Lam, J. W. Y.; Cheng, L.; Chen, H.; Qiu, C.; Kwok, H. S.; Zhan, X.; Liu, Y.; Zhu, D.; Tang, B. Z. Aggregation-Induced Emission of 1-Methyl-1,2,3,4,5-Pentaphenylsilole. *Chem. Commun.* **2001**, *18*, 1740−1741.
(32) Hong, Y.; Lam, J. W. Y.; Tang, B. Z. Aggregation-Induced Emission: Phenomenon, Mechanism and Applications. *Chem. Commun.* **2009**, *29*, 4332−4353.
(33) Yuan, W. Z.; Lu, P.; Chen, S.; Lam, J. W. Y.; Wang, Z.; Liu, Y.; Kwok, H. S.; Ma, Y.; Tang, B. Z. Changing the Behavior of Chromophores from Aggregation-Caused Quenching to Aggregation-Induced Emission: Development of Highly Efficient Light Emitters in the Solid State. *Adv. Mater.* **2010**, *22*, 2159−2163.
(34) Chen, S.; Hong, Y.; Liu, Y.; Liu, J.; Leung, C. W. T.; Li, M.; Kwok, R. T. K.; Zhao, E.; Lam, J. W. Y.; Yu, Y.; Tang, B. Z. Full-Range Intracellular pH Sensing by an Aggregation-Induced Emission-Active Two-Channel Ratiometric Fluorogen. *J. Am. Chem. Soc.* **2013**, *135*, 4926−4929.
(35) Hong, Y.; Lam, J. W. Y.; Tang, B. Z. Aggregation-Induced Emission. *Chem. Soc. Rev.* **2011**, *40*, 5361−5388.
(36) Yuan, Y.; Zhang, C.-J.; Gao, M.; Zhang, R.; Tang, B. Z.; Liu, B. Specific Light-Up Bioprobe with Aggregation-Induced Emission and Activatable Photoactivity for the Targeted and Image-Guided Photodynamic Ablation of Cancer Cells. *Angew. Chem., Int. Ed.* **2015**, *54*, 1780−1786.
(37) Kwok, R. T. K.; Leung, C. W. T.; Lam, J. W. Y.; Tang, B. Z. Biosensing by Luminogens with Aggregation-Induced Emission Characteristics. *Chem. Soc. Rev.* **2015**, *44*, 4228−4238.
(38) Leung, C. W. T.; Hong, Y.; Chen, S.; Zhao, E.; Lam, J. W. Y.; Tang, B. Z. A Photostable AIE Luminogen for Specific Mitochondrial Imaging and Tracking. *J. Am. Chem. Soc.* **2013**, *135*, 62−65.
(39) Li, J.; Liu, K.; Han, Y.; Tang, B. Z.; Huang, J.; Yan, Y. Fabrication of Propeller-Shaped Supra-amphiphile for Construction of Enzyme-Responsive Fluorescent Vesicles. *ACS Appl. Mater. Interfaces* **2016**, *8*, 27987−27995.
(40) Gu, X.; Zhao, E.; Zhao, T.; Kang, M.; Gui, C.; Lam, J. W. Y.; Du, S.; Loy, M. M. T.; Tang, B. Z. A Mitochondrion-Specific Photoactivatable Fluorescence Turn-On AIE-Based Bioprobe for Localization Super-Resolution Microscope. *Adv. Mater.* **2016**, *28*, 5064−5071.
(41) Chen, L.-J.; Ren, Y.-Y.; Wu, N.-W.; Sun, B.; Ma, J.-Q.; Zhang, L.; Tan, H.; Liu, M.; Li, X.; Yang, H.-B. Hierarchical Self-Assembly of Discrete Organoplatinum(II) Metallacycles with Polysaccharide via Electrostatic Interactions and Their Application for Heparin Detection. *J. Am. Chem. Soc.* **2015**, *137*, 11725−11735.
(42) Fan, Z.; Li, D.; Yu, X.; Zhang, Y.; Cai, Y.; Jin, J.; Yu, J. AIE Luminogen-Functionalized Hollow Mesoporous Silica Nanospheres for Drug Delivery and Cell Imaging. *Chem. - Eur. J.* **2016**, *22*, 3681−3685.
(43) Li, J.; Shi, K.; Drechsler, M.; Tang, B. Z.; Huang, J.; Yan, Y. A Supramolecular Fluorescent Vesicle Based on A Coordinating Aggregation Induced Emission Amphiphile: Insight into the Role of Electrical Charge in Cancer Cell Division. *Chem. Commun.* **2016**, *52*, 12466−12469.
(44) Cihlář, J. Hydrolysis and Polycondensation of Ethyl Silicates. 1. Effect of pH and Catalyst on the Hydrolysis and Polycondensation of Tetraethoxysilane (TEOS). *Colloids Surf., A* **1993**, *70*, 239−251.
(45) De, G.; Karmakar, B.; Ganguli, D. Hydrolysis-Condensation Reactions of TEOS in the Presence of Acetic Acid Leading to the Generation of Glass-Like Silica Microspheres in Solution at Room Temperature. *J. Mater. Chem.* **2000**, *10*, 2289−2293.
(46) Mazumdar, P.; Das, D.; Sahoo, G. P.; Salgado-Moran, G.; Misra, A. Aggregation Induced Emission Enhancement of 4,4[Prime or Minute]-Bis(Diethylamino)Benzophenone with an Exceptionally Large Blue Shift and Its Potential Use as Glucose Sensor. *Phys. Chem. Chem. Phys.* **2015**, *17*, 3343−3354.
(47) Chen, C.; Ke, J.; Zhou, X. E.; Yi, W.; Brunzelle, J. S.; Li, J.; Yong, E.-L.; Xu, H. E.; Melcher, K. Structural Basis for Molecular Recognition of Folic Acid by Folate Receptors. *Nature* **2013**, *500*, 486−489.
(48) Low, P. S.; Henne, W. A.; Doorneweerd, D. D. Discovery and Development of Folic-Acid-Based Receptor Targeting for Imaging and Therapy of Cancer and Inflammatory Diseases. *Acc. Chem. Res.* **2008**, *41*, 120−129.
(49) Santra, S.; Kaittanis, C.; Santiesteban, O. J.; Perez, J. M. Cell-Specific, Activatable, and Theranostic Prodrug for Dual-Targeted Cancer Imaging and Therapy. *J. Am. Chem. Soc.* **2011**, *133*, 16680−16688.
(50) Mosmann, T. Rapid Colorimetric Assay for Cellular Growth and Survival: Application to Proliferation and Cytotoxicity Assays. *J. Immunol. Methods* **1983**, *65*, 55−63.
(51) Carmichael, J.; DeGraff, W. G.; Gazdar, A. F.; Minna, J. D.; Mitchell, J. B. Evaluation of A Tetrazolium-Based Semiautomated Colorimetric Assay: Assessment of Radiosensitivity. *Cancer Res.* **1987**, *47*, 943−946.
(52) Kalbáčová, M.; Verdánová, M.; Mravec, F.; Halasová, T.; Pekař, M. Effect of CTAB and CTAB in the Presence of Hyaluronan on Selected Human Cell Types. *Colloids Surf., A* **2014**, *460*, 204−208.
(53) Lai, J.; Shah, B. P.; Garfunkel, E.; Lee, K.-B. Versatile Fluorescence Resonance Energy Transfer-Based Mesoporous Silica Nanoparticles for Real-Time Monitoring of Drug Release. *ACS Nano* **2013**, *7*, 2741−2750.
(54) Clapp, A. R.; Medintz, I. L.; Uyeda, H. T.; Fisher, B. R.; Goldman, E. R.; Bawendi, M. G.; Mattoussi, H. Quantum Dot-Based Multiplexed Fluorescence Resonance Energy Transfer. *J. Am. Chem. Soc.* **2005**, *127*, 18212−18221.
(55) Xue, X.; Zhao, Y.; Dai, L.; Zhang, X.; Hao, X.; Zhang, C.; Huo, S.; Liu, J.; Liu, C.; Kumar, A.; Chen, W.-Q.; Zou, G.; Liang, X.-J. Spatiotemporal Drug Release Visualized through a Drug Delivery

DOI: 10.1021/acsami.7b06306
ACS Appl. Mater. Interfaces 2017, 9, 21706−21714

System with Tunable Aggregation-Induced Emission. *Adv. Mater.* **2014**, *26*, 712−717.
(56) Wang, T.; Chai, F.; Fu, Q.; Zhang, L.; Liu, H.; Li, L.; Liao, Y.; Su, Z.; Wang, C.; Duan, B.; Ren, D. Uniform Hollow Mesoporous Silica Nanocages for Drug Delivery *in vitro* and *in vivo* for Liver Cancer Therapy. *J. Mater. Chem.* **2011**, *21*, 5299−5306.
(57) Yang, X.; Grailer, J. J.; Pilla, S.; Steeber, D. A.; Gong, S. Tumor-Targeting, pH-Responsive, and Stable Unimolecular Micelles as Drug Nanocarriers for Targeted Cancer Therapy. *Bioconjugate Chem.* **2010**, *21*, 496−504.
(58) Morais, E. C.; Correa, G. G.; Brambilla, R.; Radtke, C.; Baibich, I. M.; Santos, J. H. Z. d. The Interaction of Encapsulated Pharmaceutical Drugs with a Silica Matrix. *Colloids Surf., B* **2013**, *103*, 422−429.
(59) Harada, A.; Ono, M.; Yuba, E.; Kono, K. Titanium Dioxide Nanoparticle-Entrapped Polyion Complex Micelles Generate Singlet Oxygen in the Cells by Ultrasound Irradiation for Sonodynamic Therapy. *Biomater. Sci.* **2013**, *1*, 65−73.
(60) Tada, H.; Shiho, O.; Kuroshima, K.-i.; Koyama, M.; Tsukamoto, K. An Improved Colorimetric Assay for Interleukin 2. *J. Immunol. Methods* **1986**, *93*, 157−165.
(61) Gieni, R. S.; Li, Y.; HayGlass, K. T. Comparison of [3H]Thymidine Incorporation with MTT- and MTS-Based Bioassays for Human and Murine IL-2 and IL-4 Analysis Tetrazolium Assays Provide Markedly Enhanced Sensitivity. *J. Immunol. Methods* **1995**, *187*, 85−93.

DOI: 10.1021/acsami.7b06306
ACS Appl. Mater. Interfaces 2017, 9, 21706−21714